AIP | Review of Scientific Instruments

Photoacoustic spectroscopy applied to the study of clay soils

D. R. dos Santos, R. Toledo, M. S. O. Massunaga, J. G. Carrió, L. T. Auler, E. C. da Silva, A. Garcia-Quiroz, and H. Vargas

Citation: Review of Scientific Instruments **74**, 355 (2003); doi: 10.1063/1.1518553

View online: http://dx.doi.org/10.1063/1.1518553

View Table of Contents: http://scitation.aip.org/content/aip/journal/rsi/74/1?ver=pdfcov

Published by the AIP Publishing

Photoacoustic spectroscopy applied to the study of clay soils

D. R. dos Santos, R. Toledo, M. S. O. Massunaga, J. G. Carrió, and L. T. Auler
LCFIS–UENF, Avenida Alberto Lamego 2000, Campos dos Goytacazes, RJ 28015-620, Brazil

E. C. da Silva and A. Garcia-Quiroz
IFGW–UNICAMP Caixa Postal 6165, Campinas, SP 13083-970, Brazil

H. Vargas[a)]
LCFIS–UENF, Avenida Alberto Lamengo 2000, Campos dos Goytacazes, RJ 28015-620, Brazil

(Presented on 24 June 2002)

The optical absorption spectra and mineralogical composition of soil samples were characterized using photoacoustic spectroscopy and x-ray diffraction. The photoacoustic spectra observed showed transition bands associated with Fe^{3+} ions in octahedral or tetrahedral symmetry. From the phase behavior, both the nonradiative relaxation time τ and the characteristic thermal diffusion time τ_β were determined. The x-ray diffraction analysis showed that kaolinite is a major crystalline phase (86 wt %) followed by minor quantities of anatase, gibbsite, and quartz. Rietveld refinements showed that the Fe^{3+} cations partially substitute for Al^{3+} cations in octahedral sites of the kaolinite structure. © *2003 American Institute of Physics.* [DOI: 10.1063/1.1518553]

I. INTRODUCTION

Clay minerals have a large variety of applications, including industrial processes, agriculture, environmental remediation, and construction. The physical and chemical properties of a particular clay mineral, such as particle size and shape, surface area and charge, degree of substitution, color, viscosity, plasticity, porosity, and water absorption are responsible for their specific applications. Kaolinite is classified as a two-layer clay, i.e., a sheet of silica tetrahedra combined through octogonal hydroxyls which are shared with an alumina octahedral sheet. This highly crystalline structure has little substitution of other elements, but there may be some Fe substituting for Al, which results in red pigmentation after firing.

In this work a systematic study on selected raw materials used by ceramic industries is presented. Soil samples were obtained from a large sedimentary basin at the northern Rio de Janeiro state, Brazil. The ceramic industry is growing economically in this region, and careful evaluation of the kaolin deposits must be made. In previous work the thermal properties of the soil clay fraction were determined, and it was shown that thermal diffusivity, heat capacity, and thermal conductivity are very sensitive to the amorphous-crystalline phase transition that occurs when the samples are heated above 950 °C, which is a temperature typically applied in the manufacturing process to obtain ceramic materials with desirable performance.[1]

The economic value of the ceramic product is also affected by its red pigmentation, which is mainly due to the presence of oxides, hydroxides, and hydrated oxides of ferric iron. These iron oxides that occur in soil either as coatings on individual clay particles, or as discrete, fine particles throughout the clay mass, can be removed by organic acids[2] or by chemical reduction of the iron to ferrous form.[3]

Photoacoustic spectroscopy (PAS) was applied to study the optical absorption spectra of clay soils which is related to the Fe content and its valence state. In addition, a quantitative phase analysis was performed using the Rietveld method[4] and major mineral phases were identified.

II. EXPERIMENTAL PROCEDURES

The soil samples were dried, ground, and passed through a sieve with a nominal aperture of 74 μm (mesh 200).

The PAS experiments were performed using a spectrometer consisting of a 1000 W xenon arc lamp the radiation of which was modulated by a variable speed chopper (SRS, model SR540). A monochromator in combination with appropriate absorption filters was used for wavelength selection and to eliminate higher order effects. The beam leaving the monochromator was directed into a conventional PA cell, a small gas-tight enclosure with a condenser microphone (Bruel and Kjaer, model 4165) mounted in one wall. Changes in sample temperature cause alterations of the pressure in the enclosed gas which are subsequently converted to an electrical signal by the microphone. The signal was preamplified and fed to a lock-in amplifier (SRS, model SR830), connected to a microcomputer. Loading of the cell was accomplished via an attachable sample holder, with the powder placed in an open cavity. The PAS signal was divided by the signal obtained from carbon black in order to eliminate the spectral variation of the illumination source.

X-ray powder diffraction (XRD) data were acquired in Bragg–Brentano geometry using Cu $K\alpha$ radiation by a conventional diffractometer (Seifert URD65) equipped with a graphite diffracted beam monochromator. The XRD data were collected in the angular range of $3° \leqslant 2\theta \leqslant 70°$ in steps of 0.02° and a 5 s counting time.

[a)]Electronic mail: vargas@uenf.br

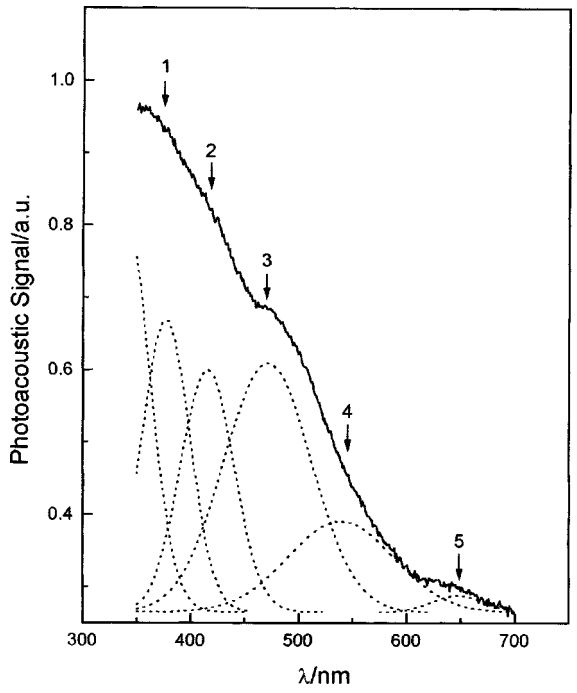

FIG. 1. Typical photoacoustic spectrum of soil samples. The arrows indicate the positions of the absorption bands and dotted lines correspond to deconvolution of the experimental curve.

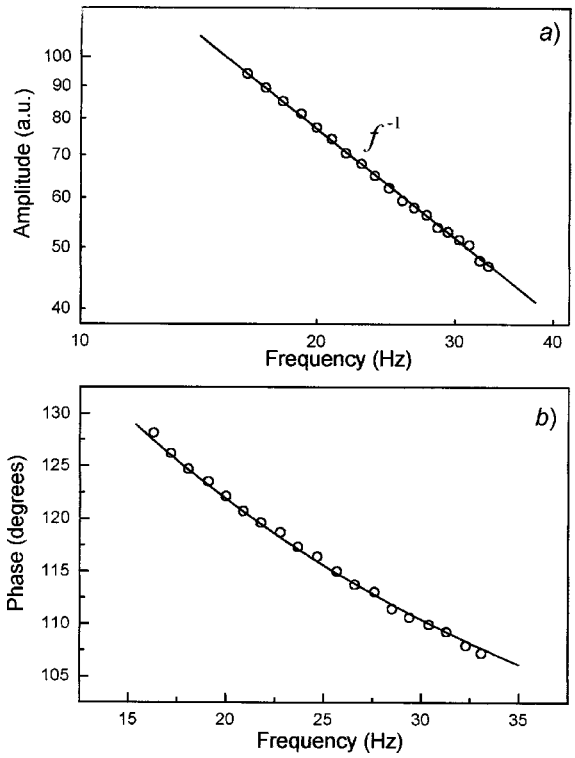

FIG. 2. (a) Amplitude of the photoacoustic signal vs modulation frequency at 490 nm. The solid line corresponds to a linear fit to the data, which on a logarithmic scale represents a f^{-1} power law. (b) Phase of the photoacoustic signal (dots). The solid line corresponds to the data fit [Eq. (3) of the text].

III. RESULTS AND DISCUSSION

A. Photoacoustic spectroscopy

Figure 1 shows a typical PA spectrum of the soil samples recorded at a chopping frequency of 20 Hz. The arrows, 1–5, indicate the position of spectral bands associated with the electronic transitions of the Fe^{3+} from the $^6A_1(^6S)$ level, to, respectively, levels $^4T_1(^4G)$; $^4T_2(^4G)$; ^4E, $^4A_1(^4G)$; $^4T_2(^4D)$; and $^4E(^4D)$. According to ligand field theory these transitions are expected when Fe^{3+} ions are in octahedral or tetrahedral symmetry.[5] The same behavior was observed in all samples. Some band positions could not be easily identified. In Fig. 1, for example, the spectrum displays a very small shoulder at 540 nm that upon Gaussian deconvolution discloses an absorption band. In Table I the mean positions of the transition bands are listed. These results are in agreement with theoretical predictions.[6,7]

Having obtained the PA spectra, the procedure described in the paper of Lima *et al.*[8] was used to obtain the nonradiative relaxation time τ and the characteristic diffusion time τ_β for each absorption band. Figure 2(a) shows the signal's dependence on the modulation frequency for the 490 nm band. The signal exhibits f^{-1} dependence, which was also observed for the other absorption bands. This result is in contrast to the $f^{-1.5}$ frequency dependence predicted by the Rosencwaig and Gersho model[9] for a thermally thick optically transparent (unsaturated) sample, but agrees with that expected when the thermal expansion of the sample is a dominant mechanism responsible for the PAS signal. In this case the acoustic signal is proportional to the average temperature in the sample. In fact, using Rosencwaig and Gersho theory modified to include the effect of a finite nonradiative relaxation time, the pressure fluctuation δP in the PA cell is given by

$$\delta P = \frac{\gamma P_0 I_0 \alpha_t \beta l_s \exp(i\omega t)}{l_g k_s \sigma_s^2 (1-\beta/\sigma_s)(1+i\omega\tau)}, \tag{1}$$

where γ is the ratio of specific heats for air, P_0 is the ambient pressure, I_0 is the incident light intensity at a given wavelength, α_t is the thermal expansion coefficient of the sample, β is the optical absorption coefficient of the sample, l_s is the length of the sample, $\omega = 2\pi f$, where f is the modulation frequency applied, l_g is the length of the gas, k_s is the thermal conductivity of the sample, $\sigma_s = (1+i)\mu_s^{-1}$ is the complex thermal diffusion coefficient, $\mu_s = (2\alpha_s/\omega)^{1/2}$ is the thermal diffusion length of the sample, $\alpha_s = k_s/\rho_s c_s$ is the thermal diffusivity of the sample, and τ is the nonradiative relaxation time for the sample.

We notice that Eq. (1) holds for a thermally thick optically transparent sample, namely, $l_s\sigma_s \gg 1$ and $\beta l_s \ll 1$. Information about τ and τ_β is obtained from measurements of the thermal wave phase angle ϕ as a function of the modulation frequency. In the thermally thick region of our experiment, these parameters are calculated from Eq. (1), by writing it as $\delta P = |\delta P| \exp[i(\omega t + \phi)]$, where

TABLE I. Position λ, nonradiative relaxation time τ, and the characteristic diffusion time τ_β for each absorption band.

Band	1	2	3	4	5
λ (nm)	370	430	490	540	650
τ (ms)	5.9	6.2	6.5	6.7	7.2
τ_β (μs)	0.13	0.13	0.12	0.16	0.20

$$|\delta P| = \frac{\gamma P_0 I_0 \alpha_t \beta l_s \alpha_s}{l_g k_s \omega [(1-\beta\mu_s/2)^2 + (\beta\mu_s/2)^2]^{1/2} [1+(\omega\tau)^2]^{1/2}}, \tag{2}$$

and

$$\phi = -\frac{\pi}{2} - \tan^{-1}(\omega\tau) - \tan^{-1}\left(\frac{1}{(2\omega\tau_\beta)^{1/2}-1}\right), \tag{3}$$

where $\tau_\beta = (\beta^2 \alpha_s)^{-1}$. Equation (2) implies that, provided $\beta\mu_s < 1$, the PAS amplitude is proportional to both the optical absorption coefficient and to the thermal expansion coefficient and that it varies as f^{-1} for $\omega\tau \ll 1$. The latter condition is normally fulfilled well whereas the first condition requires that the thermal diffusion length, μ_s, is much smaller than the optical penetration depth, β^{-1}, a condition that is satisfied well for the samples studied within the modulation frequency range of our experiment. The dependence of the PAS phase on the modulation frequency, Eq. (3), has been used by several authors to study the behavior of τ and τ_β in collisional deactivation of vibrational excitation in gases, polymers, and in the nonradiative relaxation of dopant ions in crystal and glasses.[9,10]

Figure 2(b) shows typical results for the PAS phase obtained at 490 nm. The data fitting results for each absorption band are summarized in Table I. The values of τ (about 6.5 ms) are in very close agreement for all absorption bands. Note that the relaxation time τ measured photoacoustically is not necessarily that appropriate to the level initially excited in the absorption process, but rather to the average lifetime of a variety of states before energy is lost as heat. Furthermore, for powder samples τ also contains a contribution from a heat exchange time between the powder particles and the transducing gas in the PA cell. This heat exchange time depends not only on the shape of the particles but also on their size. The fact that τ values remain very close for all bands suggests that this heat exchange time dominates the nonradiative relaxation process. The values of τ_β, on the other hand, exhibit large discrepancies. The reason for this is the sensitivity of the phase angle ϕ with respect to τ_β. As pointed by Baesso *et al.*,[10] the variation of ϕ given by Eq. (3) is quite insensitive to the value of τ_β in the low modulation frequency region, thereby leading to poor accuracy in the values of τ_β obtained from the phase resolved method.

B. X-ray diffraction

All soil samples presented very similar results. A quantitative phase analysis was performed using the Rietveld method with the DBWS program[4] and Fig. 3 shows the Rietveld fitting for one typical powder diffractogram. The results indicate kaolinite as the main phase (85.8 wt %), followed by quartz (5.5%), anatase (5.2%), and gibbsite (3.6%). Iron oxides such as hematite, magnetite, and illmenite were not detected. Atomic positions, cell parameters, site occupation factors and texture were refined for kaolinite. Structural parameters of the minor phases were not refined. Taking into account the importance of the presence of iron ions detected by the PAS technique, the possibility of Al^{3+} substitution by Fe^{3+} cations in the octahedral sites of the kaolinite structure was considered. Significant improvement of the quality of the was achieved by substituting 50% of the Al^{3+} ions by Fe^{3+} ions.

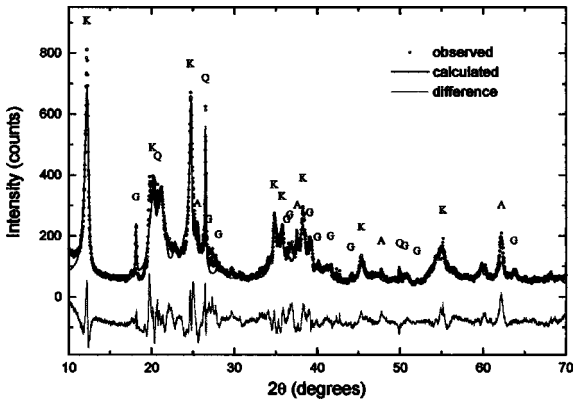

FIG. 3. Powder diffractogram and the result of Rietveld refinement for quantitative phase analysis. Peaks corresponding to each crystalline phase are K (kaolinite), Q (quartz), G (gibbsite), and A (anatase).

IV. CONCLUSIONS

The x-ray diffraction analysis showed that the main crystalline phase present in the soil samples studied is kaolinite (86 wt %) followed by minor quantities of anatase, gibbsite, and quartz. Rietveld refinements showed that Fe^{3+} cations partially substitute for Al^{3+} cations in the octahedral sites of the kaolinite structure.

The PAS analysis showed transition bands associated with Fe^{3+} ions in tetrahedral or octahedral symmetry. From the phase behavior, both the nonradiative relaxation time τ and the characteristic thermal diffusion time τ_β were determined. Very similar values of τ (about 6.5 ms) were obtained for all absorption bands, suggesting that the heat exchange time between the powder particles and the transducing gas dominates the nonradiative relaxation process. The values of τ_β, on the other hand, exhibit large discrepancies due to the poor sensitivity of the phase angle ϕ with respect to τ_β in the low modulation frequency region.

ACKNOWLEDGMENTS

The authors acknowledge CNPq and FAPERJ for their financial support.

[1] J. Alexandre, F. Saboya, B. C. Marques, M. L. P. Ribeiro, C. Salles, M. G. da Silva, M. S. Sthel, L. T. Auler, and H. Vargas, Analyst **124**, 1209 (1999).
[2] V. R. Ambikadevi and M. Lalithambika, Appl. Clay Sci. **16**, 133 (2000).
[3] O. P. Mehra and M. L. Jackson, Clays Clay Miner. **7**, 317 (1960).
[4] R. A. Young, A. Sakthivel, T. S. Moss, and C. O. Paiva-Santos, J. Appl. Crystallogr. **28**, 366 (1995).
[5] S. Sugano, Y. Tunabe, and H. Kamimura, *Multiplets of Transition-Metal Ions in Crystals* (Academic, New York, 1970).
[6] T. Abritta and F. de Souza Barros, J. Lumin. **40**, 187 (1988).
[7] T. Abritta, N. Cella, and H. Vargas, Chem. Phys. Lett. **161**, 12 (1989).
[8] G. A. R. Lima, M. L. Baesso, Z. P. Arguello, E. C. da Silva, and H. Vargas, Phys. Rev. B **36**, 9812 (1987).
[9] A. Rosencwaig and A. Gersho, J. Appl. Phys. **47**, 64 (1976).
[10] M. L. Baesso, A. M. Mansanares, E. C. da Silva, and H. Vargas, Phys. Rev. B **40**, 1880 (1989).